Guangyan Shen
Graduate

Zhonghui Xiao
Graduate

Wen Zhang
Professor

Tiesheng Zheng[1]
Professor
e-mail: zhengts@fudan.edu.cn

Department of Mechanics and
Engineering Science,
Fudan University,
Shanghai 200433, P. R. China

Nonlinear Behavior Analysis of a Rotor Supported on Fluid-Film Bearings

A fast and accurate model to calculate the fluid-film forces of a fluid-film bearing with the Reynolds boundary condition is presented in the paper by using the free boundary theory and the variational method. The model is applied to the nonlinear dynamical behavior analysis of a rigid rotor in the elliptical bearing support. Both balanced and unbalanced rotors are taken into consideration. Numerical simulations show that the balanced rotor undergoes a supercritical Hopf bifurcation as the rotor spin speed increases. The investigation of the unbalanced rotor indicates that the motion can be a synchronous motion, subharmonic motion, quasi-period motion, or chaotic motion at different rotor spin speeds. These nonlinear phenomena are investigated in detail. Poincaré maps, bifurcation diagram and frequency spectra are utilized as diagnostic tools.
[DOI: 10.1115/1.2149394]

1 Introduction

Fluid-film bearings play a key role in the design of turbomachinery systems. They are important components of turbines, compressors, and pumps that are widely used in aircraft, naval ship as well as petrochemical, power and petroleum industries. In these bearings, the fluid-film provides a means to support loads and attenuate frictions.

The fluid-film forces are highly nonlinear functions of journal displacement and velocity. The bearings behave in a strongly nonlinear fashion and significantly affect the dynamic behaviors of the system. This leads to subharmonic, quasi-periodic and chaotic motions of the rotor. In 1978, Holmes [1] published the first paper about the aperiodic behavior in journal bearings. Bently [2] reported the experimental observations of the second and third order subharmonic vibrations. Furthermore, Ehrich observed subharmonic vibration [3,4] and chaotic vibration phenomenon [5] in high-speed rotor dynamic systems. Based on these findings, turbo machinery manufacturers and users started to realize that the nonlinearities within rotor systems might have significant local and global effects on their behavior. This is particularly the case with present high performance designs, which call for higher speeds and reliability in increasingly compact configurations. The dynamical behavior of the systems must be investigated by nonlinear theory instead of the conventional linear theory. Using linearized coefficients causes a complete loss of information about nonlinear phenomena such as subharmonic, quasi-periodic, and chaotic motions that can only be predicted by the original nonlinear equations. In addition, another limitation of the linear theory is that the linear rotordynamic coefficients yield stability information only for a balanced rotor. Even so, they are unable to determine if the bifurcation is subcritical or supercritical. For example, the linearized stability criterion of a static equilibrium point suggests that machines should not be operated beyond the threshold speed of instability. However, there have been several cases shown that machines were virtually stable far beyond the threshold speeds of instability [6]. These kinds of phenomena due to nonlinearities within rotor bearing systems can only be explained through nonlinear instability analysis.

One of the most difficult obstacles in the nonlinear analysis of rotor-bearing systems is how to calculate the fluid-film forces fast and accurately. In general, the calculation of the fluid-film forces requires solving the Reynolds equation. The film pressure is solved from the Reynolds equation by applying appropriate boundary conditions and then integrating over the journal area to get the fluid forces. Solving the Reynolds equation is tedious for a whirling journal since pressures have to be calculated at each instant of time. Excessive computation time is often required to obtain steady state responses, particularly if they are chaotic. The most accurate but, at the same time, the most time-consuming methods are the finite element method (FEM) [7–11] and the finite difference method (FDM) [12–14]. Since the fluid-film force sometimes needs to be calculated more than ten thousand times to obtain the steady state responses, FEM and FDM are too time-consuming in nonlinear behavior analysis. By omitting some terms, the Reynolds equation yields special forms for short journal bearings ($L/D \ll 1$) [15,16] or long journal bearings ($L/D \gg 1$) [17,18]. Both short and long bearing approximations yield analytical solutions for the pressure distributions and hence for fluid-film forces. The analytical solutions of fluid-film forces bring much convenience to the instability analysis. Therefore, most nonlinear behavior analyses of rotor-bearing system used the short bearing theory [19–22] or the long bearing theory [23]. There is, however, no analytical solution for fluid-film forces of the multilobe bearings commonly used in practice. In particularly, it becomes more complicated to get the analytical solution when applying the Reynolds boundary condition, which reduces the defect of the Sommerfeld boundary condition and the Gümbel boundary condition.

This paper presents a new model to calculate the fluid-film forces under the Reynolds boundary condition and applies this model to investigate the nonlinear dynamics of a rigid rotor in the elliptical bearing support. Both balanced and unbalanced rotors are considered herein. Hopf bifurcation of the balanced rotor; synchronous and periodic, quasi-periodic, and chaotic motions of the unbalance rotor are also shown. Poincaré maps, bifurcation diagram and frequency spectra are selected as diagnostic tools.

2 Motion Equations of Rigid Rotor

Figure 1 shows a rigid journal rotating in a fixed elliptical bearing housing which consists of two 150 deg arch pads. O_j is the geometric center of the journal, O_b is the geometric center of the bearing; and O_b–xy is the fixed Cartesian coordinates system.

[1]Corresponding author.

Contributed by the Technical Committee on Vibration and Sound of ASME for publication in the JOURNAL OF VIBRATION AND ACOUSTICS. Manuscript received November 5, 2003; final manuscript received July 14, 2005. Assoc. Editor: George T. Flowers.

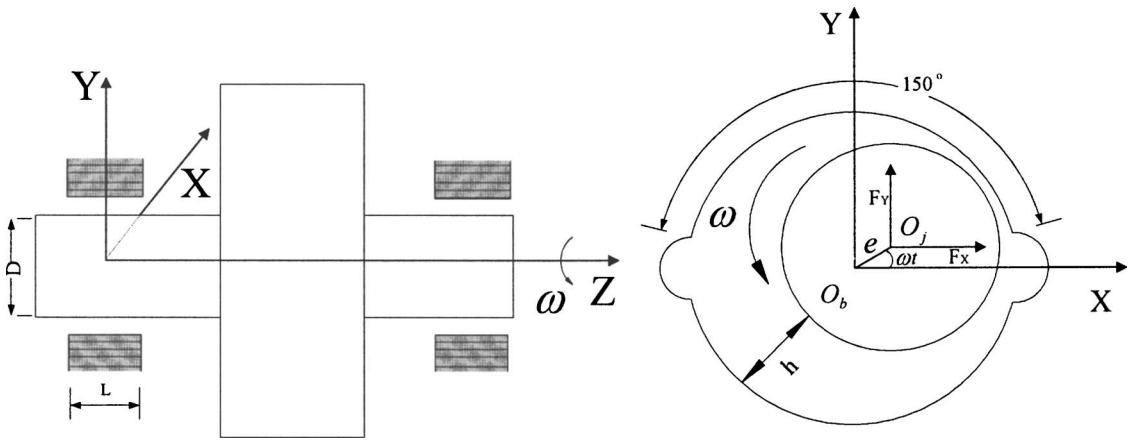

Fig. 1 Model of the rotor supported by two elliptical bearings

To simplify the analysis, only the parallel radial motion of rotor is considered. The equations of the motion of journal center O_j can be written as

$$mX'' = F_X(X,Y,X',Y') + me\omega^2 \cos \omega t$$

$$mY'' = F_Y(X,Y,X',Y') + me\omega^2 \sin \omega t - mg \tag{1}$$

Equation (1) has the following dimensionless form:

$$mC\omega^2\ddot{x} = \frac{6\mu\omega {R_b}^4}{C^2} f_x(x,y,\dot{x},\dot{y}) + me\omega^2 \cos \tau$$

$$mC\omega^2\ddot{y} = \frac{6\mu\omega {R_b}^4}{C^2} f_y(x,y,\dot{x},\dot{y}) + me\omega^2 \sin \tau - mg \tag{2}$$

Introducing the dimensionless rotating speed $\sigma=\omega\sqrt{e/g}$, eccentricity to clearance ratio $\rho=e/C$ and combined parameter $\kappa=6\mu {R_b}^4/mC^3\cdot\sqrt{e/g}$, Eq. (2) can be rewritten as

$$\ddot{x} = \frac{\kappa}{\sigma} f_x(x,y,\dot{x},\dot{y}) + \rho \cos \tau$$

$$\ddot{y} = \frac{\kappa}{\sigma} f_y(x,y,\dot{x},\dot{y}) + \rho\left(\sin \tau - \frac{1}{\sigma^2}\right) \tag{3}$$

A new model of calculating the fluid-film forces f_x, f_y is shown in the next section.

3 Calculate the Fluid-film Forces

Figure 2 represents the cross section of the journal bearing in local coordinates and the pad in circular cylindrical coordinates. The pad domain Ω is separated into two sets $\Omega=\Omega^+\cup\Omega^0$.

The fluid-film forces can be obtained by integrating the pressure p over the area of the journal sleeve. The pressure distribution p of one pad can be calculated as follows.

Based on the variational inequality theory [24], the problem of solving the pressure under Reynolds boundary condition can be interpreted as a minimization problem of the convex set. When all non-negative smooth functions satisfy the external boundary conditions, the pressure p is shown to be a function which minimizes the energy integral:

$$J(p) = \min_{q\in K} J(q) \tag{4}$$

where

$$J(q) = \frac{1}{2}\int\int_\Omega h^3\left[\left(\frac{\partial q}{\partial\theta}\right)^2 + \left(\frac{\partial q}{\partial\zeta}\right)^2\right] d\theta d\zeta - \int\int_\Omega f\cdot q d\theta d\zeta \tag{5}$$

$$h = 1 - u\cos\theta - v\sin\theta \tag{6}$$

$$f = (-u + 2\dot{v})\sin\theta + (v + 2\dot{u})\cos\theta \tag{7}$$

$$K = \{q \in c^1(\Omega) | q \geqslant 0 \text{ in } \Omega, \text{and } q = 0 \text{ on } \partial\Omega\} \tag{8}$$

Recall that Ω^+ is approximately a rectangular domain and the value of the pressure is very close to zero near the boundary, the pressure can be denoted as

$$q(\theta,\zeta) = g(\zeta)r(\theta) \tag{9}$$

Equation (5) can, therefore, be written as

$$J(q) = \tfrac{1}{2}(c_1 d_1 + c_2 d_2) - c_3 d_3 \tag{10}$$

where

$$c_1 = \int_{-\lambda}^{\lambda} g^2(\zeta)d\zeta, \quad c_2 = \int_{-\lambda}^{\lambda} g'^2(\zeta)d\zeta, \quad c_3 = \int_{-\lambda}^{\lambda} g(\zeta)d\zeta \tag{11}$$

$$d_1 = \int_0^\gamma h^3(\theta)r'^2(\theta)d\theta, \quad d_2 = \int_0^\gamma h^3(\theta)r^2(\theta)d\theta,$$

$$d_3 = \int_0^\gamma f(\theta)r(\theta)d\theta \tag{12}$$

Therefore, if $r(\theta)$ is obtained, we can obtain the following Euler-Lagrange equation by minimizing Eq. (4):

$$d_2 g''(\zeta) - d_1 g(\zeta) = -d_3, \quad g(-\lambda) = g(\lambda) = 0 \tag{13}$$

The solution of Eq. (13) gives $g(\zeta)=b[\cosh(k\lambda)-\cosh(k\zeta)]$, where

$$k = \sqrt{d_1/d_2} \tag{14}$$

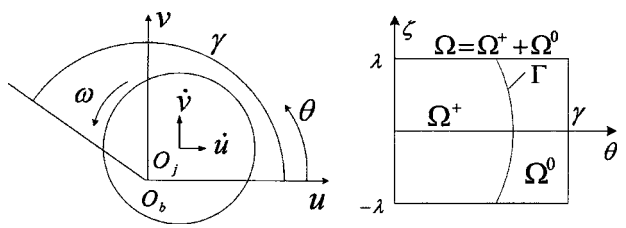

Fig. 2 Cross section of journal and one pad of bearing in local coordinates

Let $b \cdot r(\theta) \Rightarrow r(\theta)$, without losing generality, $g(\zeta)$ becomes

$$g(\zeta) = \cosh(k\lambda) - \cosh(k\zeta) \tag{15}$$

Equation (11) can, therefore, be written as

$$c_1 = 2\lambda + \lambda \cosh(2k\lambda) - \frac{3}{2k}\sinh(2k\lambda)$$

$$c_2 = \frac{k}{2}[\sinh(2k\lambda) - 2k\lambda]$$

$$c_3 = \frac{2}{k}[k\lambda \cosh(k\lambda) - \sinh(k\lambda)] \tag{16}$$

Set k to be an initial value. Since the values of c_1, c_2, and c_3 are determined, the minimization problem (4) can be reduced to a one-dimensional problem, i.e., finding a function

$$r(\theta) \in \{c^1[0,\gamma] | r(\theta) \geqslant 0 \text{ in } (0,\gamma) \text{ and } r(0) = r(\gamma) = 0\} \tag{17}$$

to minimize

$$J(r) = \frac{1}{2}\int_0^\gamma h^3(\theta)[c_1 r'^2(\theta) + c_2 r^2(\theta)]d\theta - c_3\int_0^\gamma f(\theta) r(\theta) d\theta \tag{18}$$

According to Eq. (14), k can be updated during the process of the calculation. Numerical examples show that k converges rapidly and the result is insensitive to the initial value of k.

In order to search for the approximate solution of $r(\theta)$, let us first introduce a parameter $0 < \delta \leqslant \gamma$ and a normalized variable $0 \leqslant \eta = \theta/\delta \leqslant 1$. Consequently, $r(\theta)$ can be interpolated by using Lagrange polynomial and yield

$$r(\theta) = \begin{cases} r(\eta) = w(\eta) \cdot \boldsymbol{l}^T(\eta)\boldsymbol{a}, & \text{while } 0 \leqslant \eta \leqslant 1 \\ 0, & \text{other cases} \end{cases} \tag{19}$$

where

$$\boldsymbol{a} = \{a_i\}_{i=1,n}^T, \quad \boldsymbol{l}(\eta) = \{l_i(\eta)\}_{i=1,n}^T, \quad l_i(\eta) = \prod_{j=1,\neq i}^{n} \frac{\eta - \eta_j}{\eta_i - \eta_j} \tag{20}$$

and $\eta_i = (i-1)/(n-1)$, $(i = 1, \ldots, n)$ are the basic interpolation points and $l_i(\eta)$, $(i = 1, \ldots, n)$ are the bases of the Lagrange polynomial. The high order polynomial interpolation is seldom used in practice due to poor numerical stability. In this paper, the weight function $w(\eta)$ in Eq. (19) is used to make the low order interpolation more accurate. In fact, very accurate results for $r(\theta)$ are obtained by three-order polynomial interpolation with the following weight function

$$w(\eta) = h^{-2}(\delta\eta)\sin(\pi\eta) \tag{21}$$

Because $w(\eta) \geqslant 0$ and $r(\eta_j) = a_j w(\eta_j)$, $\boldsymbol{a} \geqslant 0$ means that the solution is non-negative. Furthermore, $a_n = 0$ shows $r(\delta) = r(\delta) = 0$, which satisfies the Reynolds boundary condition.

Substitute Eq. (19) into Eq. (12), yields

$$d_1 = \boldsymbol{a}^T\boldsymbol{K}_1\boldsymbol{a}, \quad d_2 = \boldsymbol{a}^T\boldsymbol{K}_2\boldsymbol{a}, \quad d_3 = \boldsymbol{a}^T[(v + 2\dot{u})\boldsymbol{b}_1 + (-u + 2\dot{v})\boldsymbol{b}_2] \tag{22}$$

where

$$\boldsymbol{K}_1 = \frac{1}{\delta}\int_0^1 h^3(w'(\eta)\boldsymbol{l}(\eta) + w(\eta)\boldsymbol{l}'(\eta))(w'(\eta)\boldsymbol{l}(\eta) + w(\eta)\boldsymbol{l}'(\eta))^T d\eta$$

$$\boldsymbol{K}_2 = \delta\int_0^1 h^3 w^2(\eta)\boldsymbol{l}(\eta)\boldsymbol{l}^T(\eta) d\eta \tag{23}$$

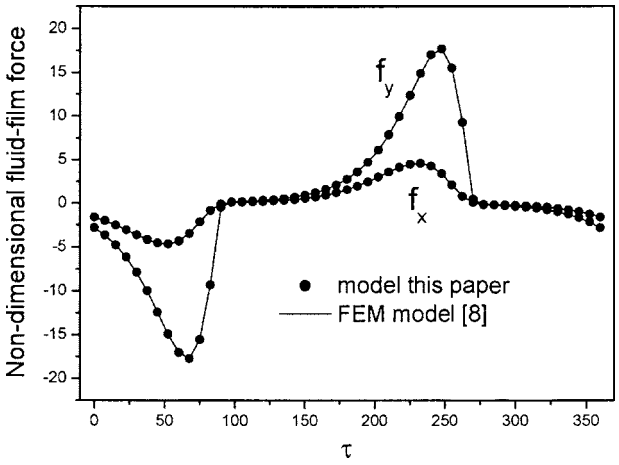

Fig. 3 Comparison of the fluid-film force between two methods

$$\boldsymbol{b}_1 = \delta\int_0^1 \cos\frac{\eta}{\delta} w(\eta)\boldsymbol{l}(\eta) d\eta, \quad \boldsymbol{b}_2 = \delta\int_0^1 \sin\frac{\eta}{\delta} w(\eta)\boldsymbol{l}(\eta) d\eta \tag{24}$$

Therefore Eq. (18) yields:

$$J(r) = \tfrac{1}{2}\boldsymbol{a}^T\boldsymbol{K}\boldsymbol{a} - \boldsymbol{a}^T\boldsymbol{b} \tag{25}$$

where

$$\boldsymbol{K} = c_1\boldsymbol{K}_1 + c_2\boldsymbol{K}_2, \quad \boldsymbol{b} = c_3[(v + 2\dot{u})\boldsymbol{b}_1 + (-u + 2\dot{v})\boldsymbol{b}_2] \tag{26}$$

Obviously, Eq. (25) is minimum when

$$\boldsymbol{a} = \boldsymbol{K}^{-1}\boldsymbol{b} \tag{27}$$

The parameter δ is determined by following the iterations. First set $\delta = \gamma$. If the solution of Eq. (27) satisfies $\boldsymbol{a} \geqslant \boldsymbol{0}$, it means the fluid-film fills the whole pad. Thus, the solution of $r(\theta)$ can be obtained directly. If the solution gives $a_n < 0$, then cavitation appears. In the cavitation case, δ should be modified and $\boldsymbol{a}$ is recalculated iteratively until $a_n = 0$.

The fluid-film forces of one pad in local coordinates can be obtained by

$$\begin{Bmatrix} f_u \\ f_v \end{Bmatrix} = -\int_{-\lambda}^{\lambda} g(\zeta) d\zeta \int_0^\gamma r(\theta) \begin{Bmatrix} \cos\theta \\ \sin\theta \end{Bmatrix} d\theta = -c_3 \begin{Bmatrix} \mathbf{b}_1^T\mathbf{a} \\ \mathbf{b}_2^T\mathbf{a} \end{Bmatrix} \tag{28}$$

Transforming the forces to global coordinates and summing for all of the pads gives the bearing forces f_x and f_y

4 Nonlinear Dynamic Analysis

In this paper, both rigid balanced and unbalanced rotors in elliptical bearing supports are investigated (Fig. 1). The value of the parameters for the example are $R_j = 0.1$(m), $m = 100$(kg), $\mu = 0.02$(Pa·s), $C/R_j = 0.003$, $C_{\min}/C = 0.5$, and $\lambda = 1.0$. Since the fluid-film forces are calculated pad by pad, the present method is effective not only on cylindrical bearings, but also on multilobe bearings, including the elliptical form.

Because the accuracy of the fluid-film force will subsequently change the numerical values of the nonlinear rotor simulation, a validation for the proposed method is conducted. The fluid-film forces of the elliptical bearings are obtained by setting up $C/R_j = 0.003$, $C_{\min}/C = 0.5$ and $\lambda = 1.0$. A comparison is made with the FEM in which the free boundary is determined by the complementary iteration [8] and shown in Fig. 3. Figure 3 demonstrates the fluid-film force when dimensionless displacements $x = \varepsilon\cos\tau$ and $y = \varepsilon\sin\tau$ where $\varepsilon = 0.45$, $\dot{\varepsilon} = 0$ and τ changes from 0 deg to 360 deg. The results of the current model agree very well with that

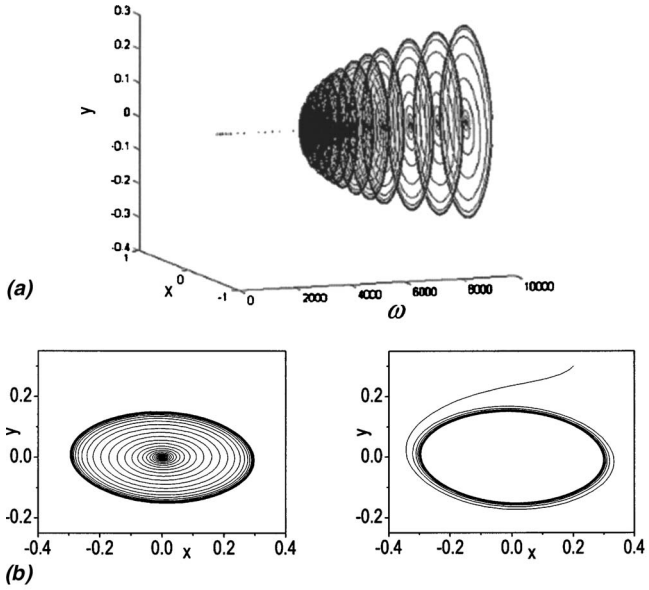

Fig. 4 Hopf bifurcation and limit circle of balanced rotor, (*a*) Hopf bifurcation; (*b*) limit circle for ω=5000

obtained by the FEM method. The maximum error occurs when τ=97.5 deg and τ=277.5 deg. The maximum relative error of $f=\sqrt{f_x^2+f_y^2}$ is 3.6%. However, the present model works much more efficiently than the FEM method by simplifying the problem from two-dimensional to one-dimensional. The computational time consumed for the present model is less than 1% of that for the FEM model.

The fast computation characteristic of the present fluid-film forces model makes numerical analysis feasible. The dimensionless Eqs. (3) are numerically integrated using a fourth-ordered Runge-Kutta method with a constant time step of $2\pi/64$. The solutions give the journal motion data, which is then used to plot the bifurcation diagram, dynamic orbit, Poincaré map, and power spectrum.

4.1 Balanced Rotor. If the mass eccentricity of the rotor is e=0, which means the absence of an unbalanced excitation, the journal reaches a static equilibrium position and spins at a constant speed. The static equilibrium position loses stability when the spin speed increases beyond a threshold point. Under such operating conditions, the hydrodynamic forces generated in fluid-film bearings are capable of sustaining self-excited oscillations in which energy is transferred from rotation of the rotor into a whirling motion, which is referred to as oil whirl. When the speed increases beyond the threshold limit, the whirl motion of the journal either gradually or suddenly becomes unbounded. We study

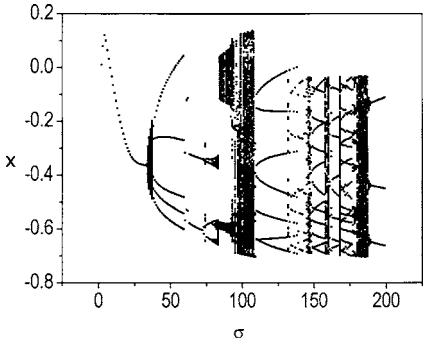

Fig. 5 Bifurcation diagram

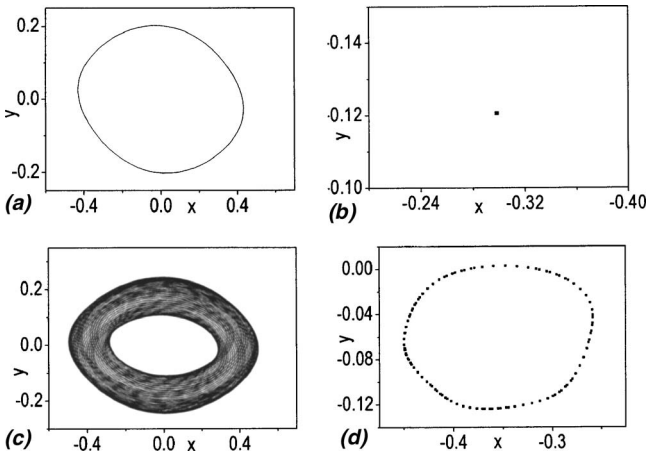

Fig. 6 Orbit and the projected Poincaré map of synchronous motion and quasi-periodic motion. (Top) Synchronous motion for σ=20; (*a*) orbit, (*b*) projected Poincaré map. (Bottom) Quasi-perodic motion for σ=35; (*c*) orbit, (*d*) projected Poincaré map

the dynamic behavior of a rotor that starts from the zero initial condition. Figure 4(*a*) shows the loci of the journal as the rotor spin speed increases. It can be observed that the rotor loses stability at ω=3800(rad/s). For the speed beyond the threshold point, Fig. 4(*b*) shows the limit circle of the rotor orbits. As rotor spin speed increases, the radius of the limit circle rises gradually, this is known as the supercritical Hopf bifurcation.

4.2 Unbalanced Rotor. In practical machines, unbalanced excitation is presented in most cases, which completely alters the

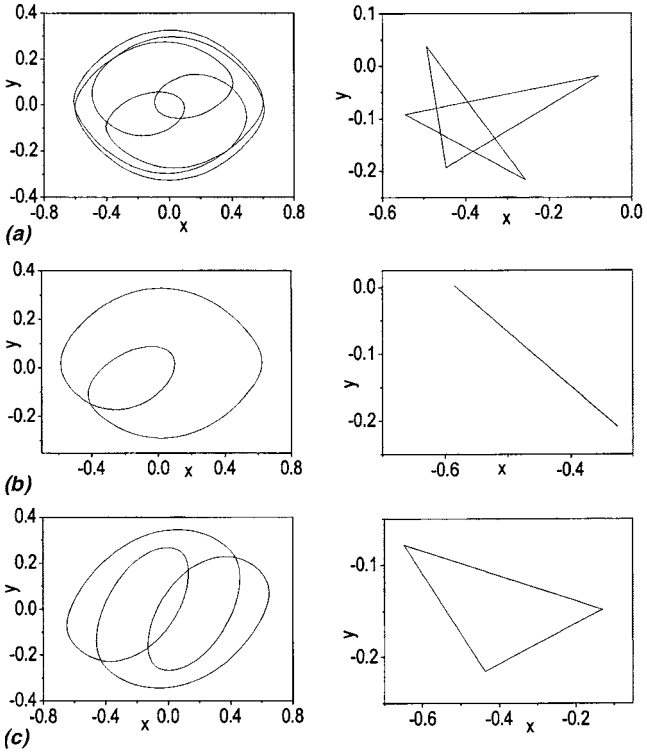

Fig. 7 Orbit and mode locking diagram of subharmonic motion. (*a*) 1/5 subharmonic motion for σ=45; (*b*) 1/2 subharmonic motion for σ=65; (*c*) 1/3 subharmonic motion for σ=190

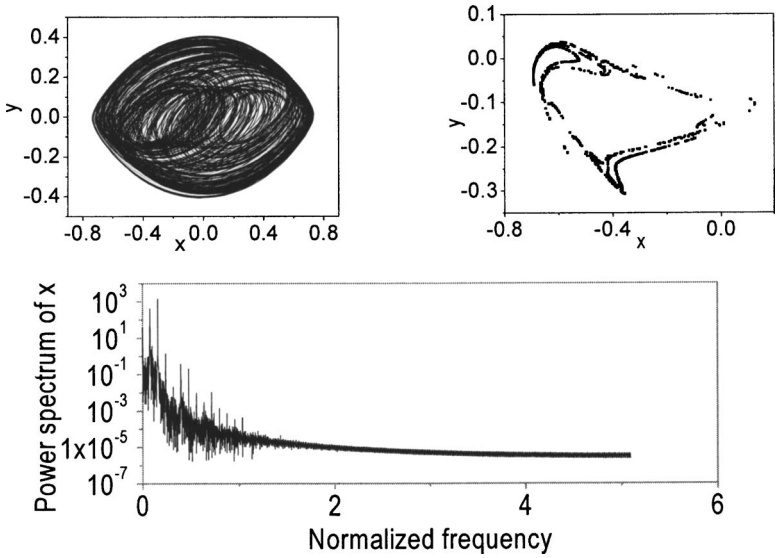

Fig. 8 The orbit of journal, projected Poincaré map, and power spectrum of journal displacement in horizontal direction of chaotic motion for σ=100

dynamics of the system [25]. Here the stability concerns the whirl orbit. Due to the complexity of the rotor motion, we selected the bifurcation diagram, dynamic orbit, Poincaré map and power spectrum as diagnostic tools. The ratio of eccentricity to clearance in this example is set to ρ=0.3.

The bifurcation diagram provides a summary of the essential dynamics; hence it is a useful way to observe nonlinear dynamical behavior. The bifurcation diagram in Fig. 5 is obtained by starting the simulation with zero initial values and the rotor speed varies with a constant step. The data of the first 500 revolutions of the rotor is not used to determine the response at steady state. The x-coordinate of the point in the Poincaré map is plotted versus the dimensionless rotor speed.

For $\sigma<33$, the motion of the journal is synchronous. When the motion is synchronous, the orbit of the journal is a single circle and there is only one point in the Poincaré map as illustrated in Fig. 6(a). At σ=33, the journal response takes on the appearance of a Neimark bifurcation to quasi-periodic motion, as illustrated with the orbit and the projected Poincaré map of Fig. 6(b) at speed σ=35. In the case of quasi-periodic motion, the points appear to fill up a closed curve in the Poincaré map. The quasi-periodic motion os maintained until σ=37. Then, the journal orbit becomes period-5 motion from σ=37 to σ=60.

At σ=61, the journal response undergoes a flip bifurcation to period-2 motion. Both the period-5 motion and the period-2 motion are subharmonic motions, in which the ratio of the forced frequency and the response frequency become rational. It is also called phase locking or mode locking [26]. The orbits of these subharmonic motions and mode locking diagrams are shown in Fig. 7. The period-2 motion holds until σ=74. With $74<\sigma<84$, the journal undergoes a series of bifurcations and then quasi-periodic motion with a whirl frequency of about half of the rotating speed appears. At σ=92, chaotic motion appears, as illustrated in Fig. 8 with a geometrically fractal structure in the projected Poincaré map and a broadband FFT spectrum at speed σ=100. As the rotating speed sequentially increases, several quasi-periodic motions and various types of period motion occur. The journal response goes to chaotic motions once more when σ increases to 180 and finally returns to the period-3 motion at σ=189.

5 Conclusions

This paper presents a fast and accurate model to calculate the fluid-film forces of a fluid film bearing. Since the model is semi-analytical, it can be applied to many kinds of bearings, such as cylindrical bearings, partial arc bearings and multilobe bearings. It is not only applicable for short bearings and long bearings, but for finite length bearings as well. In this paper, a detailed investigation of the nonlinear behavior of a rigid rotor in the elliptical bearing support is demonstrated. Both the balanced and unbalanced rotors are taken into consideration. Hopf bifurcation, subharmonic motion, quasi-period motion, and chaotic motion of the rotor are studied. At present, since most analysts rely upon numerical procedures to obtain simulations of nonlinear rotor systems, a more efficient numerical method of the fluid-film forces is required so as to characterize the dynamics of nonlinear rotor systems efficiently. The usage of the present fluid-film force model allows rapid assessment of bearing performance over a relatively large bearing design range with minimal computational effort.

Acknowledgment

This research was supported by the key project of the National Natural Science Foundation (19990510) and the Key Basic Research Special Fund (G1998020361) of China.

Nomenclature

C = R_b-R_j=clearance
$C_{\min}$ = minimal clearance
D = diameter of the journal
e = mass eccentricity of the rotor
$f_u(u,v,\dot{u},\dot{v}), f_v(u,v,\dot{u},\dot{v})$ = dimensionless fluid-film forces in local coordinates, respectively
$F_X(X,Y,X',Y')$ = fluid-film force in horizontal-direction
$F_Y(X,Y,X',Y')$ = fluid-film force in vertical-direction
$f_x(x,y,\dot{x},\dot{y})$ = $F_X/(6\mu\omega R_b{}^4/C^2)$ = horizontal dimensionless fluid-film force
$f_y(x,y,\dot{x},\dot{y})$ = $F_Y/(6\mu\omega R_b{}^4/C^2)$ = vertical dimensionless fluid-film force
L = width of the journal
m = half mass of the rotor
p = dimensionless fluid-film pressure
R_b = radius of the pad arch
R_j = radius of the journal

u, v = dimensionless displacement in local coordinates

$\dot{u}, \dot{v}$ = dimensionless velocity in local coordinates

X, Y = horizontal and vertical displacement of the journal respectively

X', Y' = horizontal and vertical dimensionless velocity of the journal respectively

$x = X/C$ = horizontal dimensionless displacement of the journal

$\dot{x} = X'/C\omega$ = horizontal dimensionless velocity of the journal

$y = Y/C$ = vertical dimensionless displacement of the journal

$\dot{y} = Y'/C\omega$ = vertical dimensionless velocity of the journal

$\tau = \omega t$

ω = rotating speed of the journal

μ = oil viscosity

$\lambda = L/D$ = width to diameter ratio

$\zeta = Z/R_b$=coordinates in the axial direction

θ = coordinates in the circumferential direction

Ω = pad domain

Ω^+ = non-negative pad domain

Ω^0 = zero pad domain

Γ = boundary between Ω^+ and Ω^0

$' = d/dt$

$. = d/d\tau$

References

[1] Holmes, A. G., Ettles, C. M., and Mayes, I. W., 1978, "Aperiodic Behaviour of a Rigid Shaft in Short Journal Bearings," Int. J. Numer. Methods Eng., **12**, pp. 695–702.

[2] Bently, D. E., 1974, "Forced Subrotative Speed Dynamic Action of Rotating Machinery," ASME Paper No. 74-PET-16.

[3] Ehrich, F. F., 1966, "Subharmonic Vibration of Rotors in Bearing Clearance," ASME Paper No. 66-MD-1.

[4] Ehrich, F. F., 1988, "High Order Subharmonic Response of High Speed Rotor in Bearing Clearance," ASME J. Vib., Acoust., Stress, Reliab. Des., **110**, pp. 695–702.

[5] Ehrich, F. F., 1991, "Some Observations of Chaotic Vibration Phenomena in High-Speed Rotor Dynamics," ASME J. Vibr. Acoust., **113**, pp. 50–57.

[6] Lund, J. W., 1987, "Review of the Concept of Dynamic Coefficients for Fluid Film Journal Bearings," ASME J. Tribol., **109**, pp. 38–41.

[7] Zheng, T., and Hasebe, N., 2000, "Nonlinear Dynamic Behaviors of a Complex Rotor-Bearing System," ASME J. Appl. Mech., **67**, pp. 485–495.

[8] Zheng, T., and Hasebe, N., 2000, "Calculation of Equilibrium Position and Dynamic Coefficients of a Journal Bearing Using Free Boundary Theory," ASME J. Tribol., **122**, pp. 616–621.

[9] Jang, G. H., and Yoon, J. W., 2002, "Nonlinear Dynamic Analysis of a Hydrodynamic Journal Bearing Considering the Effect of a Rotating or Stationary Herringbone Groove," ASME J. Tribol., **124**, pp. 297–304.

[10] Mehta, N. P., Rattan, S. S., and Gian, B., 2003, "Static and Dynamic Characteristics of Four-Lobe Pressure-Dam Bearings," Tribol. Lett., **15**(4), pp. 415–420.

[11] Sharma, S. C., Kumar, V., Jain, S. C., Sinhasan, R., and Subramanian, M., 1999, "A Study of Slot-Entry Hydrostatic/Hybrid Journal Bearing Using the Finite Element Method," Tribol. Int., **32**, pp. 185–196.

[12] Rho, B. H., and Kim, K. W., 2002, "A Study of the Dynamic Characteristics of Synchronously Controlled Hydrodynamic Journal Bearings," Tribol. Int., **35**, pp. 339–345.

[13] Rho, B. H., and Kim, K. W., 2003, "Acoustical Properties of Hydrodynamic Journal Bearings," Tribol. Int., **36**, pp. 61–66.

[14] Someya, T., 1988, *Journal-Bearing Databook*, Spinger-Verlag, Berlin, Germany.

[15] Yang, B. S., Lee, Y. H., Choi, B. K., and Kim, B. K., 2001, "Optimum Design of Short Journal Bearings by Artificial Life Algorithm," Tribol. Int., **34**(7), pp. 427–435.

[16] Rohde, S. M, and Li, D. F., 1980, "A Generalized Short Bearing Theory," ASME J. Lubr. Technol., **102**, pp. 278–282.

[17] Vance, J. M., 1988, *Rotordynamics of Turbomachinery*, Wiley, New York.

[18] Trumpler, P. R., 1966, *Design of Film Bearings*, Macmillan, New York.

[19] Brown, R. D., Addison, P., and Chan, A. H. C., 1994, "Chaos in the Unbalance Response of Journal Bearings," Nonlinear Dyn., **5**, pp. 421–432.

[20] Capone, G., and Russo, M., 1990, "Short Bearing Theory Prediction of Inertial Turbulent Journal Orbits," ASME J. Tribol., **112**, pp. 643–649.

[21] Hollis, P., and Taylor, D. L., 1986, "Hopf Bifurcation to Limit Cycles in Fluid Film Bearings," Trans. ASME, J. Tribol., **108**(2), pp. 184–189.

[22] Inayat-Hussain, J. I., Kanki, H., and Mureithi, N. W., 2003, "On the Bifurcation of a Rigid Rotor Response in Squeeze-Film Dampers," J. Fluids Struct., **17**, pp. 433–459.

[23] Myers, C. J., 1984, "Bifurcation Theory Applied to Oil Whirl in Plain Cylindrical Journal Bearings," ASME J. Appl. Mech., **51**, pp. 244–250.

[24] Rohde, S. M., and Mallister, G. T., 1975, "A Variational Formulation for a Class of Free Boundary Problems Arising in Hydrodynamic Lubrication," Int. J. Eng. Sci., **13**, pp. 841–850.

[25] Barrett, L. E., Akers, A., and Gunter, E. J., 1976, "Effect of Unbalance on a Journal Bearing Undergoing Oil Whirl," Proc. Inst. Mech. Eng., **190**, pp. 525–543.

[26] Seydel, R., 1988, *From Equilibrium to Chaos, Practical Bifurcation and Stability Analysis*, Elsevier, New York.